International Journal of Computer Information Systems and Industrial Management Applications
ISSN 2150-7988 Volume 18(2) 2026 pp. 227-246
https://doi.org/10.70917/ijcisim-2026-2417
Article

ARaNN: An Adaptive Snake-Optimized Associated Random Neural Network for Liver Cancer Detection and Classification in CT Images

S.Venkatesan

Department of Computer Science and Engineering Adhiyamaan College of Engineering Hosur 635130,
selvamvenkatesan@gmail.com

Abstract: - Liver is the largest organ of our body and the cancer that forms inside the liver cell is called Liver Cancer (LC). Many types of liver cancers are there and the most common type is known as Hepatocellular carcinoma which starts with the cell that present in the liver hepatocyte. Less common LC types are hepatoblastoma and intrahepatic cholangiocarcinoma. The detection and classification of LC is an arduous process and performing it by manually is a time overwhelming and imprecise task. Hence now-a-days artificial intelligence based approach has been used by many hospitals. In context with this, we propose a novel optimized deep learning approach known as Adaptive Snake optimization algorithm (ASA) based Associated Random Neural Network approach (ARaNN) to identify and detect LC. To begin the process, the CT scan images are pre-processed to ignore the presence of noise and to improve the contrast to predict the features effectively. Henceforth, Fuzzy Archery Learning (FAL) algorithm is applied to segment the images followed by extracting the features and detection and classification of LC using the proposed approach. Simulations are effectuated to authenticate the performance of the proposed effort. The outcomes are analyzed by the analogous study with state-of-art works and our approach surpasses all the other approaches while detecting the LC.
Keywords: -Liver cancer, Snake optimization, Associated random neural network, Fuzzy archery Learning and Gaussian filter.

1. Introduction

The liver is an essential structure that controls the way the body burns calories and is involved in generating proteins, the accumulation of glycogen in the liver, deoxidation, as well as additional processes [1]. As a result, liver illnesses pose a severe danger to the health of society, the next most frequent disease, carcinoma of the liver, is now the main reason for deaths due to cancer in both men and women. According to the moment at which it is found, there are many procedures for malignancies of the liver, these include operating on the removal of the tumor or afflicted segment, as well as loco-regional therapy. Appropriate preliminary preparation is necessary to enhance outcomes from therapy because hepatic tumors may accumulate complex circulatory pathways and disseminated features, based on computed tomography (CT) [2] examination.

Physicians currently initially section the significant liver anatomy before the surgery, specialists then maneuver into areas affected by liver damage using fine devices such as unique needle-shaped conduits for both diagnostics and operation. Adequate localization of the arteries supplying the tumors is necessary to improve eradication outcomes and lower tumor resurgence percentages, the tendency of the hepatic stream to be dependent on peripheral capillaries is crucial in this procedure for creating the operation plans. The proximity of liver tumors and hepatic arteries [3] as well as other details such as vessel measurements have a significant impact on the outcome of tumor removal.

Consequently, fragmentation of the hepatic valves, especially the small/minor vessels is essential for enhancing the effectiveness of radiation, localized treatments, and operations involving surgery. In modern medical procedures, every portion of CT imaging is physically segmented to identify the hepatic channels; surgical hepatic stream

classification [4] still is very lengthy, tiresome, and difficult. In addition, although it generates correct structural knowledge and the level of electrons for disease management, CT scans have poor small-vessel distinction, because of this; physical hepatic vessel identification is extremely hard and susceptible to specialist disputes. Thus, academics and doctors have recently become interested in establishing an automated and effective hepatic vascular differentiation [5], the malignancy of the liver has the sixth-highest prevalence of all malignancies and rates fourth in fatality worldwide. Finding the pixels that represent the liver and disease areas in diagnostic pictures is the difficult part of the hepatic and ailment classification problem [6].

The topic of liver and tumor resection has gotten much interest, it is a vital structure that carries out essential tasks such as creating protein, steroid purification, blood screening for contaminants, creation of biological substances required for digesting, and maintenance from harmful protein coagulation [7]. It lies motionless directly beneath its surface in the precise upper region of the abdominal organs, due to its strategic multifaceted role and location; the liver is overly vulnerable to many illnesses. The overall survival rate at five years for those with the initial stages of malignancy of the liver, which accounts for 43% of cases, is 36%; for cases where the disease has progressed to adjacent organs and 13% of lymph glands [8] liver from grass-fed livestock like chicken or cattle is thought to be helpful for cancer sufferers.

This is a result of its elevated vitamin B12 concentration and substantial nutritional density, the nature of the negative consequences varies on a medical condition, the course of medication, and overall well-being, restlessness, diminished hunger, abdominal discomfort, and dropping pounds are some of the greatest typical complications for those suffering from cancer. For liver tumor categorization, several existing methodologies were suggested they attains few limitations when providing LC segmentation as well as categorization. For the patients, the benign or malignant stage of LC categorization and its treatment and precaution become challenging one. Due to the lack of data, exact finding achieve is the significant for recent researchers. By addressing these limitations, we proposed a novel SO based ARaNN for automatic identification and classification of LC from the CT scan images. The below points present the major contribution of this work.

- To remove noise and augmenting image contrast by Gaussian and median filter during liver image pre-processing and reducing the computational difficulties.
- To perform segmentation in terms of Fuzzy Archery Learning in which the tradition approach difficulties are effectively solved and perfectly segmenting LC.
- To extract shape, color and texture features from the fourth hidden layer of ARaNN and increasing the accuracy of LC detection.
- To combine adaptive snake optimization with ARaNN fines tunes the parameters thereby classifying normal liver with three classes of LC namely ICC, HCC and HB.

This part explains the remaining section of the work; the existing works of LC categorization is addressed in Section 2 and the proposed ASO with ARaNN methodology for LC classification steps are described in Section 3. Section 4 argue the experimental examination and the whole work is end up in Section 4.

2. Literature survey

Dong et al. [9] have described the Hybridized Fully Convolutional Neural Network (HFCNN) for hepatic tumor categorization, which has been quantitatively modeled to address the existing liver tumor condition. As the diagnostic and treatment strategies, the difference between cancerous and non-cancerous nodules is essential. It needs assets, knowledge, and skills of the highest caliber. Inception characteristics that were successfully extracted are blended with latent parameters and weights that had previously been in the methodology. The algorithm provided estimates of the liver capacity that were 97.22% highly precise. The investigation demonstrated the division strategy's superior precision, with a standard Dice value of 0.92. However, manual assessment and segregation take a lot of effort.

Sun et al. [10] have presented deep deep-learningmethods with just global designations, and histopathology image sorting for malignancies of the liver. These photos contain accurate cancer location comments, thus updated characteristics are taken and completely utilized to make up for this. For getting the image-level attributes for grouping, transference training is paired with multiple-instance acquisition to provide the patch-level information. The technique may be used to categorize histological pictures of a particular kind of malignancy in the liver or alternative

kinds of illness, adding further evidence in favor of individualized therapies. Thus, the strategy put forward here addresses the manipulation of massive amounts of pictures and the lack of data to train.

Yan et al. [11] have implemented a deep neural network for segmenting liver channels, it uses distinctive structures to determine the precise vascular anatomy of the liver. Additionally, creating cascading remaining-like linkages inside an individual rump interferes with, which is crucial for successfully connecting individual capillary artery segments in tandem. To accurately extract the related characteristics from feature levels, it continually picks the proper setting aspects from superficial characteristics under the guidance of advanced features. Hence, optimizing the quality of separation represents a significant difficulty.

Tran et al. [12] have modified the Un -Net model to an interconnected structure with n layers, the convergence devices' results are used to determine the disregard connectivity. The element design changes the bypassed conjunction route, combining direction, and up-convolution route. All the resultant attributes of the most recent processing component of the elements are utilized as the starting point for the ones that follow and the decryption component in the traditional method. The resultant characteristics of the earlier inversion devices have been disregarded. The liver division outcomes obtained 96.45%, and the tumor identification outcomes obtained 73.34%. Moreover, it is not suitable for more medical division of pictures.

Devi et al. [13] have evaluated an automatic Computer-Aided Diagnosis (CAD) system that participates in an essential function in getting a diagnosis of liver illness to lower the mortality incidence from malignancies of the liver. Autonomous division of the liver and abnormality identification is done in the initial stage. The innovative contrast-based feature-difference technique is then used to classify inflammation of the liver into aggressive and harmless. According to strength and appearance, the affected region's retrieved characteristics are compared to the underlying healthy organ tissue. The aforementioned variance has improved the precision by 98.6%. Thus, it is inadequate for many kinds of different liver disorder diagnoses.

Zhang et al. [14] have developed a level-set framework for autonomously localizing liver tumors by combining neural networks and improved boundary detection from uncontrolled flexible c-means. To improve the picture clarity encompassing the hepatocytes and liver tumor, the CT scan wavelengths were reduced at this point in the process to fall within an agreed-upon range. The liver was initially coarse-to-finely separated to exclude non-liver components before tumor identification. It is used to improve the liver delineation and to approximately localize the liver malignancy. Hence, systems lack domain expertise and may make categorization mistakes that are difficult to understand.

Meng et al. [15] suggested an end-to-end patch-wise segmentation algorithm should concentrate on the alterations in the geographic organization of tissues that are damaged. During modeling exercises, the dimensions are constantly changed by the difference between the anticipated classification and the actual grouping. Even though investigations have demonstrated the efficacy of genital infections and organs, this claim will be contested if additional cells are present. Choosing the right stride is essential to meet the demands of rapidity and precision. However, it cannot be used to solve assignments without a progressive link.

Balagourouchetty et al. [16] highlighted an ensemble FCNet classifier that categorizes liver disease abnormalities from the profound characteristics retrieved. Before the prediction level, an accumulation of three completely interrelated layers is incorporated, and extensive characteristics from various levels of granularity taken from the outcome of each origination layer are provided as predictor data to considerably improve the ability of the learner. The outcomes of the experiment show how effective the suggested algorithm architecture is in improving reliable classification. Thus, it is difficult to address the identification of patterns.

3. Proposed Methodology

Initially, the major goal of this work is to demonstrate good segmentation, identification and classification of LC by means of optimized deep learning model. Each neural network involves the process of training and testing. Primarily, we suggested to Gaussian and median filters to filter out the noise and increases superiority of liver CT image and doing segmentation by means of fuzzy Archery optimization algorithm. At end, applying Adaptive Snake Optimization based Associated Random Neural Network (ASO-ARaNN) approach to identify and categorizes normal liver with different classes of LC namely Intrahepatic Cholangio Carcinoma (ICC), Hepato Cellular Carcinoma (HCC) and Hepato-Blastoma (HB). The pipeline of proposed work to determine LC detection and classification indicated in Figure 1.

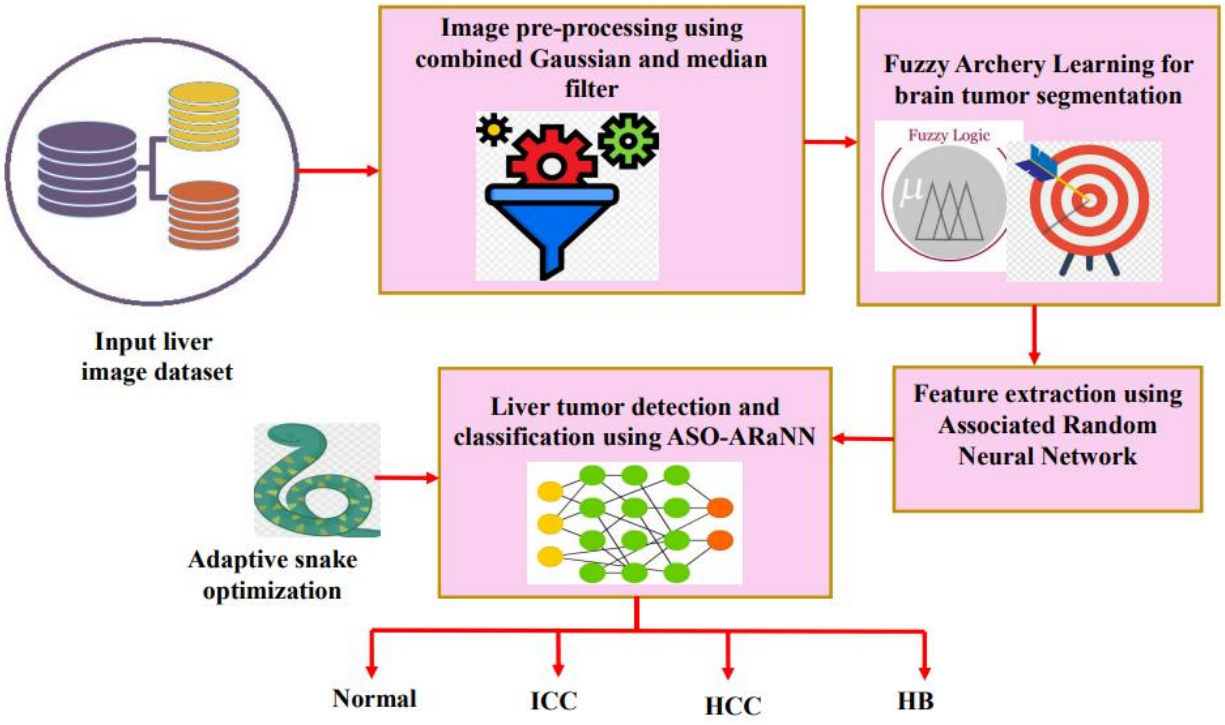

Fig. 1. The overall proposed pipeline diagram

3.1.Pre-processing

The input images are converted input the greyscale with the pixel size of 512×512 . The 1×1 window with Gaussian filter handles image pre-processing at the initial phase. After, window kernel size of 3×3 followed by median filter doing further process. Before segmentation, Gaussian filter is to ignoring random noises [17]. From the entire model, reduced the computational difficulties. When the window to the edge in an image, an unusual pixel values are not generated by median filter. During image compression, digitization and transmission of data with random as well as unwanted noises corrupt the CT images. From the liver pre-processing, the input image $Base_i(v,h)$ as the base image. In the CT images, the bright as well as dark section filter out is the major task. Below expression implement the process of threshold function.

$$T(v,h) = \begin{cases} 1, & if \quad I(v,h) > I_{mean} + D_1 \\ 0, & if \quad I(v,h) < I_{mean} - D_2 \end{cases} \tag{1}$$

The spinal region as well as chest boundary outerior cross sections are eliminated. Each contour with the external border is $N(v,h)$. From the base image, the image mask $N(v,h)$ is utilized thereby performing the operation of bitwise AND. In the image array, every pixels are multiplied and similar position mask relavant to the corresponding pixel from the base image.

3.2.LC image segmentation

To begin with the segmentation process we have utilized Archery algorithm [18] which relies on the characteristics of the archers'. The target of the member guidance is utilized for segmenting the images of LC and updates the location of the pixels. Thepopulation matrix has been generated based on the vector representation of each pixel. The matrix of the pixels are given as,

$$A=\begin{bmatrix} A_1 \\ \vdots \\ A_j \\ \vdots \\ A_M \end{bmatrix}_{M\times n} = \begin{bmatrix} a_{1,1} & \cdots & a_{1,D} & \cdots & a_{1,n} \\ \vdots & \ddots & \vdots & \iddots & \vdots \\ a_{j,1} & \cdots & a_{j,D} & \cdots & a_{j,n} \\ \vdots & \iddots & \vdots & \cdots & \vdots \\ a_{M,1} & \cdots & a_{M,D} & \cdots & a_{M,n} \end{bmatrix}_{M\times n} \tag{2}$$

The population of the image in the jth vector is taken as A_j from the pixel matrix A in the search space with the dimensionality D. the candidate solution and the number of pixels in the matrix is denoted as n and M. for each pixels the optimization problem and objective function are estimated and the estimated vector is depicted below,

$$f=\begin{bmatrix} f_1 \\ \vdots \\ f_j \\ \vdots \\ f_M \end{bmatrix}_{M\times n} = \begin{bmatrix} f(A_1) \\ \vdots \\ f(A_j) \\ \vdots \\ f(A_M) \end{bmatrix}_{M\times 1} \tag{3}$$

The objective function is *f* here and for the jth pixel the objective function is f_j. The targeted pixels from the images are deemed by using the rectangle and square page of the target panel. Moreover, the pixel population relies on the width and to detect the width of the objective function the probability of the function is used and can be evaluated as,

$$\Pr = \frac{f - f_{Worst}}{\sum_{j=1}^{M}\left(f_j - f_{Worst}\right)} \tag{4}$$

The unwanted pixels from the population are denoted as f_{Worst}. The random pixels from the search space are chosen using the archery approach. For that cumulative probability is determined as shown below,

$$P=\begin{cases} 1, & 0 \le R_{K,D}^{j} \le C_1 \\ j, & C_{j-1} < R_{K,D}^{j} \le C_1 \\ M, & C_{M-1} < R_{K,D}^{j} \le C_M \end{cases} \tag{5}$$

The selected pixel using the Archer is P and the cumulative probability of the pixel is C_1. The random number on the Dth dimensionality lies in the range of 0 and 1. The pixel location is updated using the following equation.

$$a_{j,D}^{New} = \begin{cases} a_{j,D} + rn \times \left(a_{j,D} - B \times a_{j,D}\right), & f_P < f_j \\ a_{j,d} + rn \times \left(a_{j,D} - B \times a_{P,D}\right), & Otherwise \end{cases} \tag{6}$$

$$B = rn(1+rn) \tag{7}$$

The exploitation stage is attaining the best solution nearest to the solutions and updating is performed using the leader searchability [19] and to enhance the objective function as shown below,

$$A_j^{New} = a_j + (1-2r)\cdot rn \cdot \left(1-\frac{t}{T}\right)\cdot a_j \tag{8}$$

$$A_j = \begin{cases} A_j^{New}, & f_j^{New} < f_j \\ A_j, & Otherwise \end{cases} \tag{9}$$

The new location of the pixel can be determined as A_j^{New}. The pseudocode for the proposed AL algorithm is elucidated below,

Algorithm 1: Pseudocode for the proposed AL algorithm
Start
Initilization of parameters and maximum iteration
Initialize the parametric values of *T* and *M*
For
t=1:T do
evaluate the probability function using eqn. (4)
For
j=1:M
For
D=1:n
The member selection for the guidance is performed using eqn. (5)
The new status is evalauted using eqns. (6) and (7)
End For
The local search ability of the leader algithm is updated using the eqn. (8)
The member or pixel of the jth population is updated using the eqn. (9)
End For
Save the solution obtained
End For
Return the optimal solution attained
End

3.2.1. Fuzzification process in FAL

The productivity of the segmentation is improved by using the Archery selection procedure (ASP) and learning procedure (LP). For this we utilized Mamdani's fuzzy inference [20] and mapping of input and output is made. For this nine rules are used as shown below.

- **If** the success of **archery selection** is **low** and the success of **learning phase** is **low** then the segmentation is **neutral**.
- **If** the success of **archery selection** is **low** and the success of **learning phase** is **medium**, then the segmentation is performed on **Left.**
- **If** the success of **archery selection** is **low** and the success of **learning phase** is **high**, then the segmentation is performed in the **far left**.
- **If** the success of **archery selection** is **medium** and the success of **learning phase** is **low**, then the segmentation is performed on **right**.
- **If** the success of **archery selection** is **medium** and the success of **learning phase** is **medium**, then the segmentation is performed on **Neutral**.

- **If** the success of **archery selection** is **medium** and the success of **learning phase** is **high**, then the segmentation is performed on **Left**.
- **If** the success of **archery selection** is **high** and the success of **learning phase** is **low**, then the segmentation is performed on **far right**.
- **If** the success of **archery selection** is **high** and the success of **learning phase** is **medium**, then the segmentation is performed on **right**.
- **If** the success of **archery selection** is **high** and the success of **learning phase** is **high**, then the segmentation is performed on **Neutral.**

3.3.LC identification and classification

This section explains the proposed deep random neural network for feature extraction and also this ARNN with adaptive snake optimization handles the identification as well as classification of LC images. The following section explains the detailed steps;

3.3.1. Adaptive Snake Optimization Algorithm

For improving the ARaNN we have proposed novel optimization approach known as SA and its numerical approach in terms of fighting, feeding, and mating of the snake is explained in this section. As usual this approach also employed exploitation and exploration phases with the intricate nature of the snakes [21]. The snake population is classified into male and female and is initialized randomly. Temperature is the most factor for deciding the feeding and capulatory characteristics of the snake and is expressed as,

$$Temp = Exp\left(\frac{-I_t}{Max\,I}\right) \tag{10}$$

The current iteration of the algorithm is given as I_t and the food quality (FQ) of the snake can be determined as,

$$FQ = 0.5 \times Exp\left(\frac{-I_t}{Max\,I}\right) \tag{11}$$

The essential food of the snake in the environment is represented as $FQ < 0.25$ and the exploration phase can be represented as,

$$M_{l,n}^{I_t+1} = M_{rnd,n}^{I_t+1} \pm Q_2 \times Y_n \times \left(\left(M_{\max} - M_{\min}\right) \times rnd + M_{\min}\right) \tag{12}$$

$$M_{l,F}^{I_t+1} = Y_{rnd,F}^{I_t+1} \pm Q_2 \times Y_F \times \left(\left(M_{\max} - M_{\min}\right) \times rnd + M_{\min}\right) \tag{13}$$

The location of male and female at l^{th} is defined as $M_{l,n}^{I_t+1}$ and $M_{l,F}^{I_t+1}$. The random interval is determined as (rnd) and falls under the range of 0 and 1 with the constant value $Q_2 = 0.05$. The ability of the male and female snake to find the food is represented as Y_n and Y_F. The food determination of both snake is formulated as [22],

$$X_n = Exp\left(\frac{-F_{rnd,n}}{F_{l,n}}\right) \tag{14}$$

$$X_f = Exp\left(\frac{-F_{rnd,f}}{F_{l,f}}\right) \tag{15}$$

The fitness value of the $M_{l,n}^{I_t+1}$ and $M_{l,F}^{I_t+1}$ are represented as $F_{rnd,n}$ and $F_{rnd,f}$. While determining the exploitation the food that is presented in the environment is enough and the location of the male and female can be updated as,

$$M_{l,n}^{I_t+1} = M_{rnd,n}^{I_t+1} \pm Q_3 \times Temp \times rnd \times \left(M_{food} - M_{l,f}^{I_t}\right) \tag{16}$$

The individual location of male and female is represented as $M_{l,f}$. When the temperature is lower than 0.6, and then the oppositional learning has been adopted for the fighting phase of the snake. The oppositional learning improves the convergence speed and can be used to solve the complexities. The selected oppositional can be used to choose the population variability of ASO as shown below,

$$M_{l,n,f}(t+1) = \begin{cases} \Delta_n \pm Q_3 \times f_n + rnd \times \left(\Delta_n - M_{l,n}^{best}(I_t)\right), & if \ \left(M_{l,n}^{best}(I_t) < \Delta_n\right) \\ \Delta_f \pm Q_3 \times f_f + rnd \times \left(M_{f,n}^{best}(I_t) - \Delta_f\right), & if \ \left(M_{l,n}^{best}(I_t) \geq \Delta_f\right) \end{cases} \tag{17}$$

The best location of the male and female with the fighting spirit are f_n and f_f with its respective location are $M_{l,n}^{best}$ and $M_{l,f}^{best}$. The upper and lower constraints when adopting the oppositional factor of male and female are Δ_n and Δ_f. The mating mode can be elucidated as [23],

$$M_{l,n}^{I_t+1} = M_{l,n}^{I_t} \pm Q_3 \times G_n \times rnd \times \left(H \times M_{l,f}^{I_t} - M_{l,n}^{I_t}\right) \tag{18}$$

$$M_{l,f}^{I_t+1} = M_{l,f}^{I_t} \pm Q_3 \times G_f \times rnd \times \left(H \times M_{l,n}^{I_t} - M_{l,f}^{I_t}\right) \tag{19}$$

The mating capacity of the male and female are determined as M_n and M_f. These proposed ASA can be used for the tuning of hyper parameters of the ARaNN for the classification of LC. The pseudocode of the ASA is depicted in algorithm 2.

Algorithm 2: Pseudocode for ASA

Start

Initialize the *I, Max I, M_l, and M_f*

While $(I \leq Max\, I)$

$M_{l,n}^{I_t+1} = Male\, mate$

Evaluate the fitness value of $M_{l,n}^{I_t+1}$

$M_f^{I_t+1} = Female\ mate$

Evaluate the fitness value of $M_f^{I_t+1}$

Estimate the Temp value using eqn. (10)

Estimate the FQ using the eqn. (11)

If $(FQ < 0.5)$ **then**

Evaluation of exploration phase utilizing the eqns. (12) and (13)

Else if $(FQ > 0.6)$ **then**

Evaluation of exploration phase utilizing eqn. (16)

Else

If $(rnd > 0.6)$ **then**

Estimate the fighting mode utilizing the eqn. (17)

Else

Estimate the mating mode utilizing the eqns (18) and (19)

End if

End if

End

3.3.2. Associated Random Neural Network

According to recurrent framework, link different kinds of neurons to each other that makes ARaNN. While solving problem issues, the structure of ARaNN present in hidden layers with averaged or whole pixel values of image region. There are single input layer with eight hidden layer and four output layers in ARaNN that depending upon the principle of brain. The fourth hidden layers automatically extract the multiple features from the segmented liver cancer images. Next to feature extraction, handle liver cancer identification as well as categorization and obtains the feature values of weight and bias allocated to the input layer [24]. From the features, the liver cancer classes are identified with respect to the major role of hidden layers. The selected output are conveyed with the output layer that forward and generate features. Figure 2 outlines the basic architecture of ARaNN.

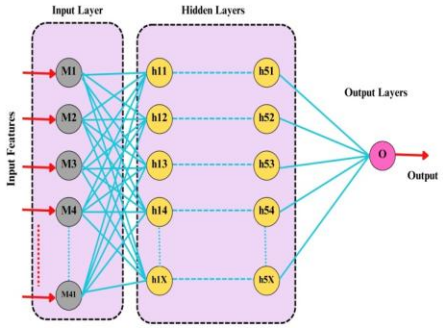

Fig. 2. General model of ARaNN

To obtain the features, the both excitation and inhibition states possess in which various layer interconnect the neurons. When there is no abnormality, an exciting state went to the neuron positive results shown by features of an images namely shape, contrast and texture. At time T, $P_i(T)$ determines neuron structure m_i that turns zero for the neuron idle value. Greater that zero, $P_i(T)$ attain the state of excitation. During the state of excitation, F_i is the rate of transmission and forward the m_i extracted feature data towards closer neuron m_j. Depending upon the probabilities $pb(i, j)$, the positive and negative data deems the forwarded features data. Below expression formulates the $v(i)$ probabilities with the neuron leave from the liver cancer extracted features [25].

$$v(i)+\sum_{j=1}^{M} pb^{pos}(i,j)+pb^{neg}(i,j)=1, \quad \forall_i \tag{20}$$

Below formula updates the neurons weight with respect to negative and positive data.

$$we^{neg}(i,j)=F_i pb^{neg}+(i,j)\geq 0 \tag{21}$$

$$we^{pos}(i,j)=F_i pb^{pos}+(i,j)\geq 0 \tag{22}$$

This study demonstrates poison distribution to analyze the probability identification for liver cancer detection. Where, $\Gamma(i)$ and $\Omega(i)$ are determines the m_i negative and positive features.

$$\Gamma^{pos}(j)=\sum_{j=1}^{m}\delta(j)\,a(j)\,pb^{pos}(j,i)+\Omega(i) \tag{23}$$

$$\Gamma^{neg}(j)=\sum_{j=1}^{m}\delta(j)\,a(j)\,pb^{neg}(j,i)+\Omega(i) \tag{24}$$

Following formula determines the function of activation and the rate of transmission.

$$\delta(j)=\frac{\Gamma^{pos}(i)}{F(i)+\Gamma^{neg}(i)} \tag{25}$$

$$F(i)=(1-v(i))^{neg}1\sum_{j=1}^{M}\left[we^{pos}(i,j)+we^{neg}(i,j)\right] \tag{26}$$

During the stage of training, update weight $F(i)$ and determines the firing rate with gain.

$$F(i)=\sum_{j=1}^{M}\left[we^{pos}(i,j)+we^{neg}(i,j)\right] \tag{27}$$

3.3.3. Associated Random Neural Network

In order to develop the ARaNN performance during the classification of LC. The number of hidden layers with the bias as well as weight functions are optimized using ASO algorithm because the ASO contains good convergence ability than other traditional optimizations [26]. It easily tunes the parameter thus demonstrating better rate of LC cataloguing. Here, ASO-ARaNN classifies various kinds of LC stages. Figure 3 plots the block diagram for the classification of LC with ASO-ARaNN model. The following points explains the steps for LC classification in terms of ASO-ARaNN.

(i) Fix M as the number of population and equally split into two groups. Select both current and maximal iterations.

(ii) To attain population based on snake's uniform distribution after the population initialization.

(iii) Initialization of optimization intervals and ARaNN hyper-parameters.

(iv) Calculate the current hyper parameters under male and female snake's individual and best fitness value.

(v) Equation (10) and (11) compute the temperature and food quality as FQ.

(vi) Equation (11) to (15) updates the individual location of male and female snakes based on spiral strategy.

(vii) Equation (16) updates the fitness value. Equation (17) updates the fighting phase of snake along with oppositional learning model.

(viii) Update the steps of mating phase. Record the individual position, replace the worst position of snake when successfully hatch the nest generation.

(ix) When the condition is satisfied decide if the maximal number of iteration met. Then, assign optimal hyper parameters to ARaNN else return the step to equation (12) for the continuation of iteration.

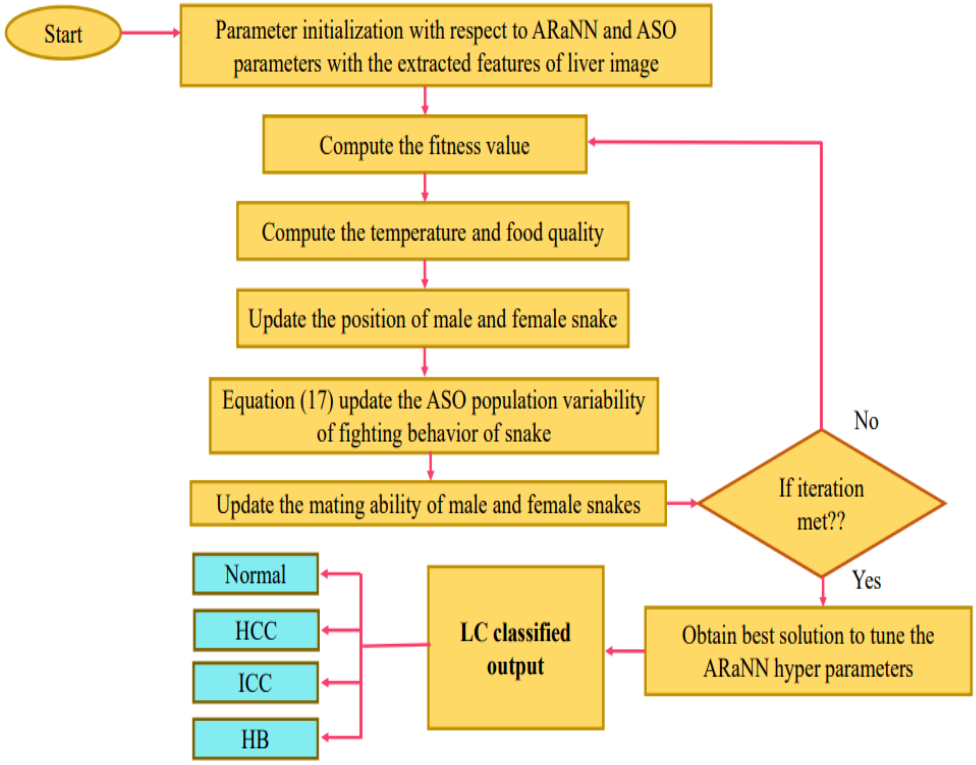

Fig. 3. LC classification using ASO-ARaNN

4. Experimental Results

The proposed framework consist of two major process such asCT image based liver tumor is segmented with FAL model as well as categorized using ASO-ARaNN model. Performance is evaluated and the process is implemented in MATLAB platform. For supervised learning, the testing and training model efficiency ensure the effectiveness of performance measures. Compare the proposed with state-of-art approaches by revealing the efficiency of proposed LC detection and categorization. Table 1 displays the explanation to simulation parameters.

Table 1. Simulation variables

Variables	Limits
Solution searching space	<0, 1>
Number of input neurons	Single
Number of hidden neurons	8
Number of output neurons	4
Activation function	ReLu
Batch size	30
Learning rate	0.001

Epoch	200
Number of population	50
Maximal amount of iteration	100

4.1. Dataset

For the conduction of LC segmentation and detection we have collected data from the famous hospital known as Medanta the Medicity, Gurgaon. This is the famous hospital with NABH and NABL certification. We have collected data from around 652 patients with different types of LC known as ICC, HCC, HB, and normal images. For recording the images the hospital utilized GE medical system with CT scan machine with the thickness of 0.5mm to 1.5mm with the resolution of 512×512. The sample images of all the four types are shown in figure 4. The figure displayed the three types of LCs such as HCC, ICC, HB, and normal images.

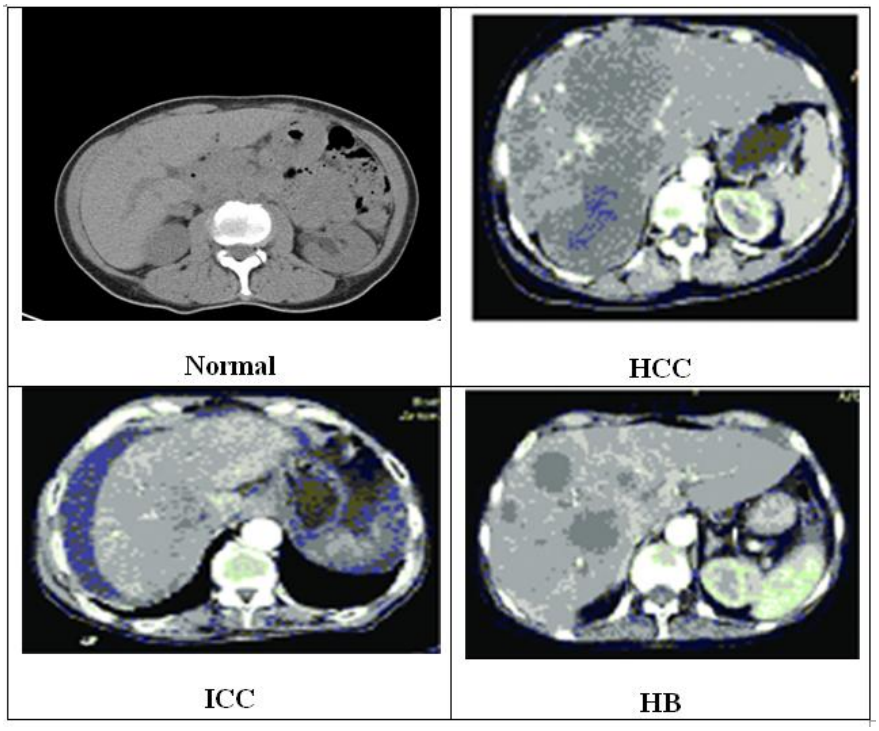

Fig. 4. Sample images collected with four namely (i) Normal Liver image, (ii) HCC LC image, (iii) ICC LC image, and (iv) HB LC image

4.2. Performance analysis based on pre-processing

The sample image results based on pre-processed outcome is as shown in Table 2. This tabulation shows the normal or healthy liver images with abnormality of LC classes namely HCC, ICC and HB for pre-processed output.

Table 2. Pre-processed results of LC sample images

Classes	Original image	Pre-processed result
Healthy (Normal)	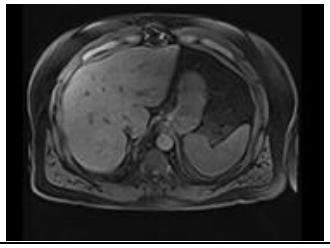	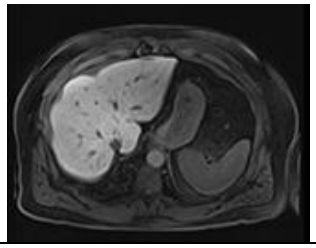

HCC	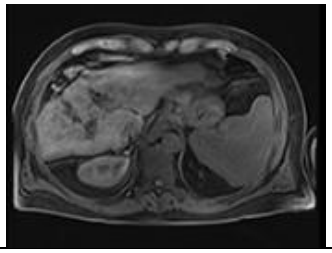	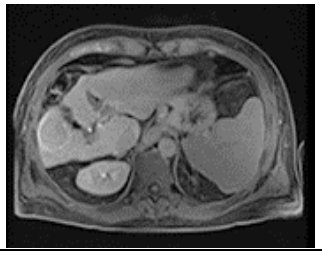
ICC	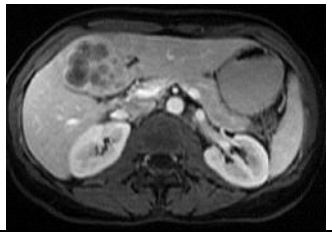	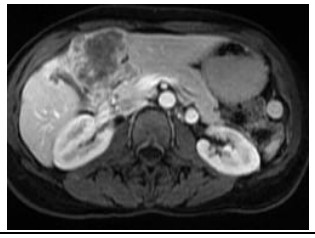
HB	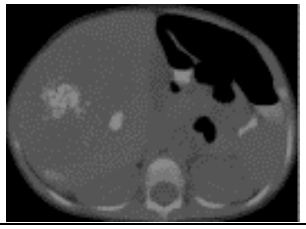	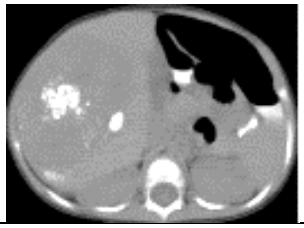

Table 3 displays the pre-processed results of above samples. The pre-processing techniques of HE, CLAHE, Gaussian flirter and proposed Gaussian with median filters with respect to the samples 1 to 4 images are illustrated by various the evaluation criteria like sensitivity, specificity and accuracy. The proposed model proves superior pre-processed outcome to other HE, CLAHE and Gaussian filter.

Table 3. Pre-processing results of an image

LC image samples	Pre-processing methods	Accuracy	Specificity	Sensitivity
Sample-1	HE	0.79	0.78	0.78
	CLAHE	0.80	0.81	0.83
	Gaussian flirter	0.85	0.86	0.87
	Gaussian with median filters	0.94	0.93	0.95
Sample-2	HE	0.70	0.73	0.74
	CLAHE	0.81	0.83	0.85
	Gaussian flirter	0.88	0.84	0.85
	Gaussian with median filters	0.95	0.94	0.96
Sample-3	HE	0.78	0.80	0.79
	CLAHE	0.84	0.86	0.87
	Gaussian flirter	0.86	0.87	0.84
	Gaussian with median filters	0.94	0.95	0.93
Sample-4	HE	0.74	0.80	0.79
	CLAHE	0.83	0.82	0.85
	Gaussian flirter	0.85	0.86	0.88
	Gaussian with median filters	0.94	0.92	0.95

4.3. Analogous study based on Segmentation of LC images

The detection LC using our proposed is effectuated using the ARaNN based ASA and prior to the classification of LC as HCC, ICC, and HB the images are segmented using proposed FAL. The segmentation outcome of our approach is higher and hence it resulted in better classification as shown in figure 5. For three sample images the segmented and classified results are depicted with respect to them.

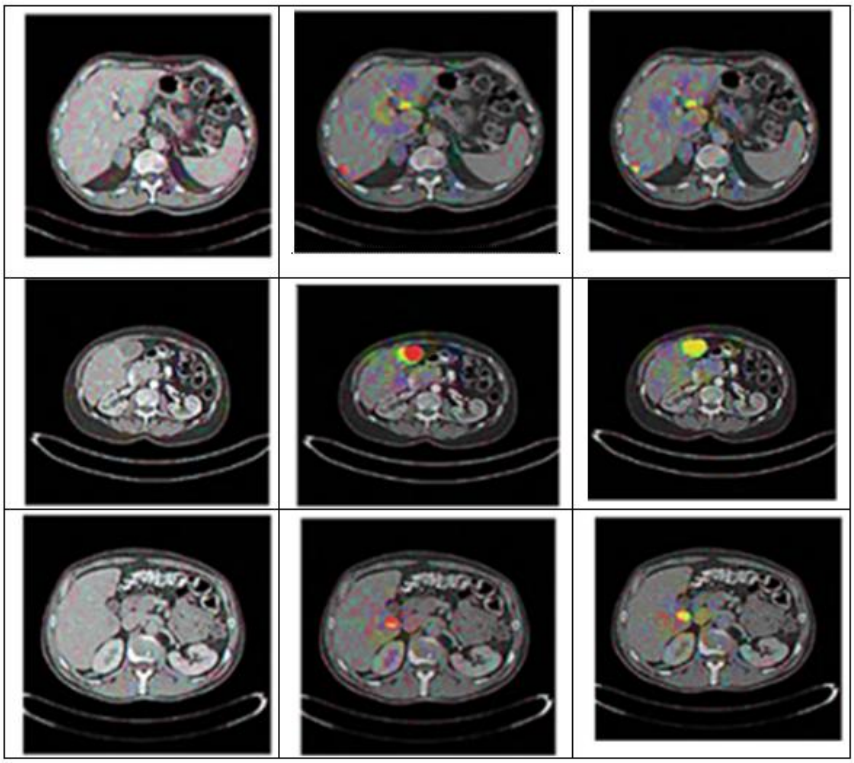

(i) (ii) (iii)

Fig. 5. Segmentation and classification results using our proposed approach (i) sample images, (ii) segmented outcome, and (iii) classified outcome

For analyzing the effectuation of proposed work we have taken some of the parameters such as Receiver Operating Characteristics (ROC), Area under the Curve (AUC), and Dice similarity coefficient. The last parameters is compared with state-of-art works such as Particle swarm algorithm based segmentation (PSO), Genetic Algorithm based segmentation (GA), Whale Optimization based segmentation (WO), and improved ant optimization based segmentation (IAO).

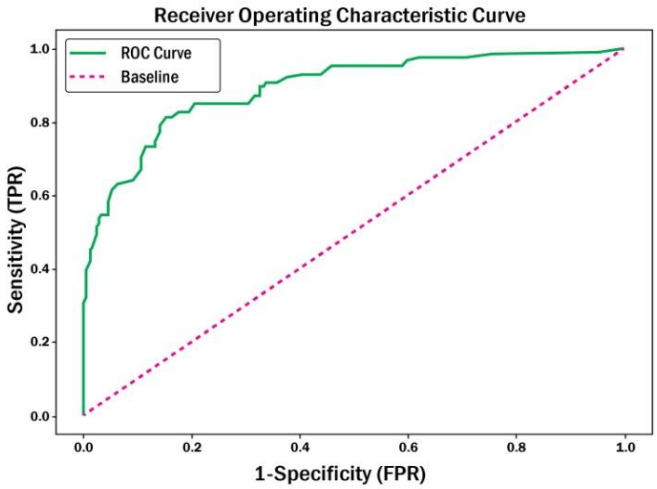

Fig. 6. Performance of proposed work in segmenting the LC images based on ROC

Our approach follows two sections (i) segmenting the liver and (ii) detecting and classifying the LC. the estimation of weights along with the pixel-wise features for all the pixels are done and the ROC of the proposed approach is visualized in figure 6. The ROC shows 0.97 with higher true positive detection and false positive rate detection.

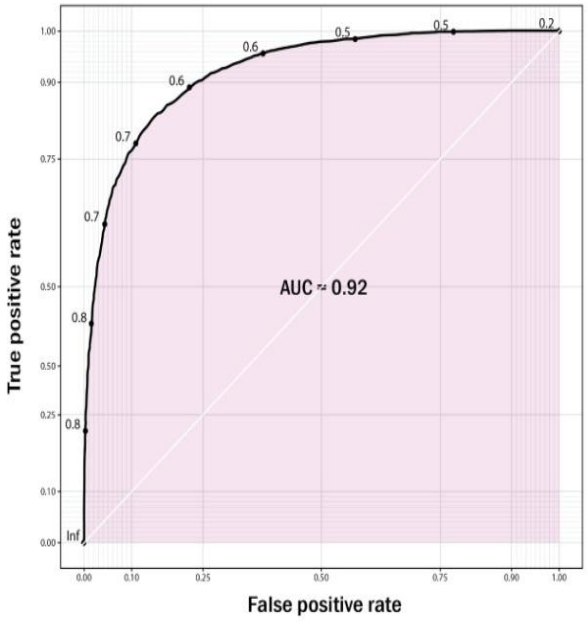

Fig. 7. Performance of proposed work in segmenting the LC images based on AUC

The AUC is used to analyze the performance of the segmentation section of LC and must lies 0 to 1. The more value depicts the better segmentation of our approach and the AUC of our proposed approach is 0.92 and effectively segments the CT scan images of LC than the other approach. The AUC of the proposed segmentation is illustrated in figure 7.

For the segmentation of any images the important parameter is the Dice similarity coefficient (DSC). Moreover, the validation of segmentation is analyzed with the result of the DSC and in this work we taken proposed and other existing approaches such as PSO, GA, WO, and IAO. The DSC is defined as,

(28)

The cardinality of the image pixel set is determined as and the value of lies between the range of 0 to 1. The value of =0 if the sets are disjointed and if it is identical the value become =1.

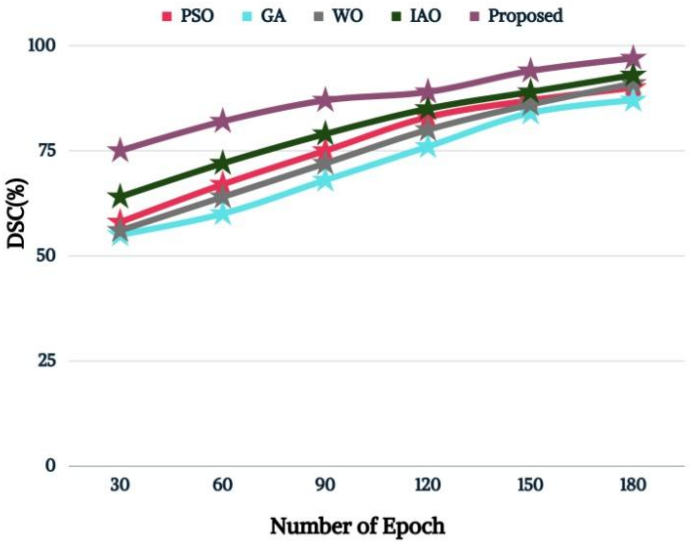

Fig. 8. Analogous study based on DSC for the segmentation of LC

The graph of the DSC for various approaches and proposed is depicted in figure 8. Here we have conducted 180 epochs and the DSC of the proposed approach is higher for all the epochs as mentioned in figure. Meanwhile, the other state-of-art works such as PSO, GA, WO, and IAO achieved lower DSC and hence the segmentation by that approaches are lower and hence the detection of LC is arduous. At 180th epoch the DSC of proposed approach is 97%, and other approaches such as PSO, GA, WO, and IAO achieved DSCs of 90%, 87%, 91%, and 93% respectively as shown in figure.

4.4. Analogous study based on classification of LC images

Figure 9 delineates the results of confusion matrix by means of healthy liver class with unhealthy LC stages such as ICC, HCC and HB. The diagonally mentions the accuracy of each class and is represented in blue colour. Depending upon this, the accuracy of 98.54%, 98.01%, 98.43% and 98.32% for normal, ICC, HCC and HB classes.

True class	Normal	ICC	HCC	HB
Normal	98.54%	1.21%	0%	0.25%
ICC	1.16%	98.01%	0.83%	0%
HCC	0.32%	0%	98.43%	1.25%
HB	0%	1.20%	0.48%	98.32%

Predicted class

Fig. 9. Confusion matrix outcome for four classes

Figure 10 shows the accuracy of LC classification by using various methods. The approximation of above 90% accuracy is accomplished by proposed method also the approximated of above 40 % results provided by existing methods such as HFCNN [9], DL [10], DNN [11] and EFCNet [16]. For comparison, the accuracy of 93%, 94%, 94.32% and 97.3% obtained in case of 50, 100, 150 and 200 iteration. However, the proposed demonstrate superior of 97.3% in 200th iteration. While classifying LC, the computational difficulties of previous methods are than that of proposed. The accuracy rate of proposed is higher in all the number of iterations compared to other HFCNN [9], DL [10], DNN [11] and EFCNet [16]. Hence, it provided good rater of classification accuracy in terms of LC.

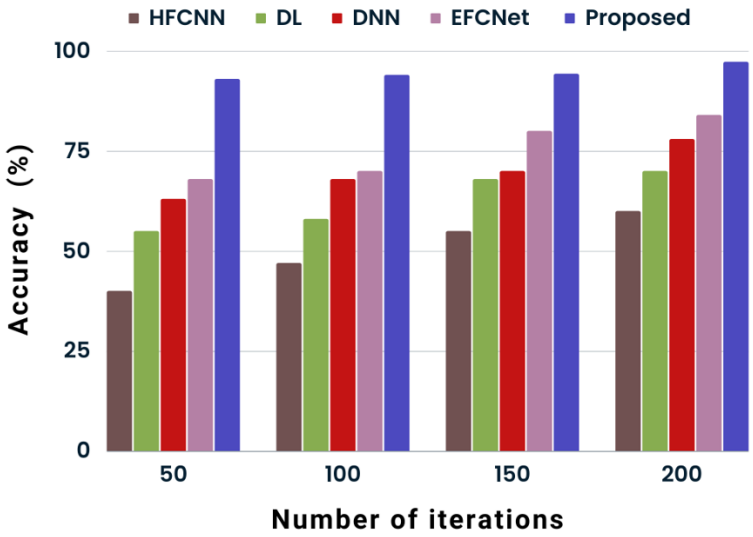

Fig. 10. Accuracy results with respect to the number of iteration

Figure 11 expose the specificity result of various methods during LC categorization. The specificity of the state-of-art method is computed to vary the number of iterations from 50 to 200 respectively. The proposed ASO-ARaNN model linked with the specificity of above 93%. The HFCNN [9], DL [10], DNN [11] and EFCNet [16] progressed to 60%, 73%, 78% and 85% specificity at the iteration of 200. To contrast by previous methodologies, the specificity of proposed ASO-ARaNN model from 50 to 200 iteration become 93%, 93.21%, 95% and 97.01% during the classification of LC image. On considering state-of-art analysis, proposed ASO-ARaNNemphasized significant simulation findings based on specificity.

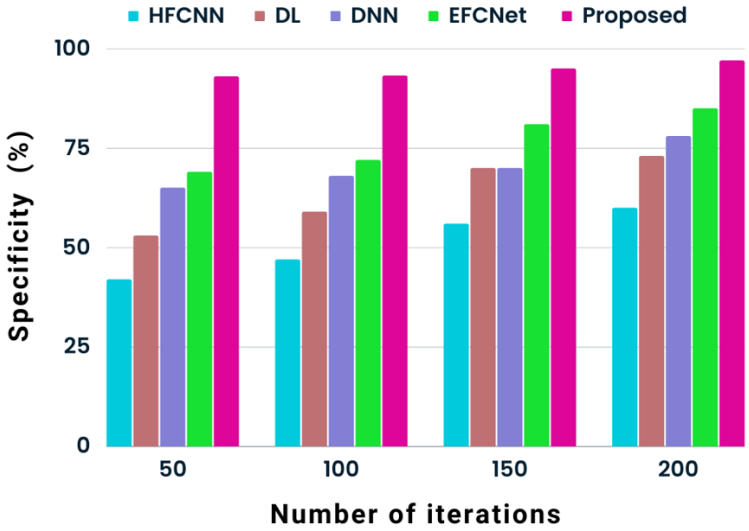

Fig. 11. Specificity results with respect to the number of iteration

Figure 12 design the schematic diagram to evaluate the sensitivity outputs. The comparative outcome of traditional methods and proposed ASO-ARaNN accomplished the sensitivity results that vary from the iteration of 50 to 200. The previousHFCNN [9], DL [10], DNN [11] and EFCNet [16] establish above 60% sensitivity results and further, an approximation of above 88% sensitivity outcomes are delineated. Depending upon 50, 100, 150 and 200 iteration, the sensitivity is 88%, 93%, 94.3% and 96.83%. Anyway, the proposed ASO-ARaNN illustrates 96.83% sensitivity in 200th iteration thereby minimizing the computational difficulties. To compare by HFCNN [9], DL [10], DNN [11] and EFCNet [16], the sensitivity of LC classification using proposed ASO-ARaNN performance is superior.

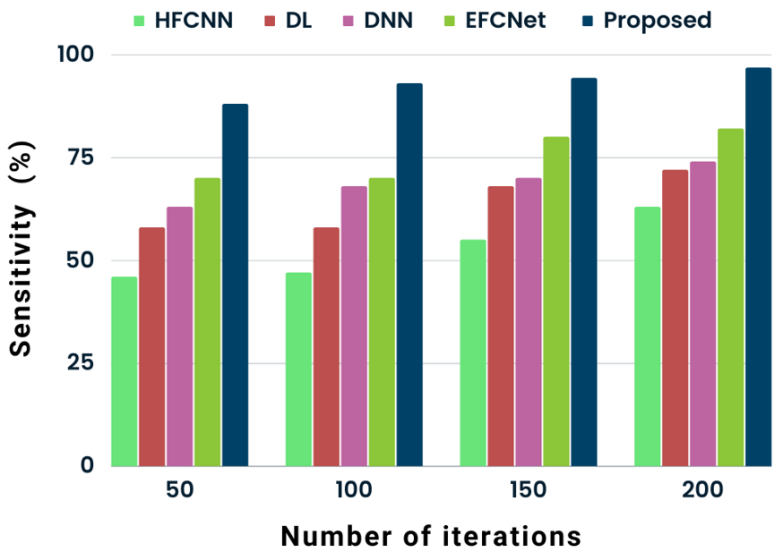

Fig. 12. Sensitivity results with respect to the number of iteration

Figure 13 explains the comparative evaluation of various optimization algorithms in terms of fitness evaluation. The traditional optimization models namely particle swarm optimization (PSO), Rat swarm optimization (RSO), Whale optimization algorithm (WOA), Grey wolf optimization (GWO) and proposed ASO algorithms are selected to show the convergence performance. By this plot, the convergence ability of proposed ASO is good than other PSO, WOA, RSO and GWO.

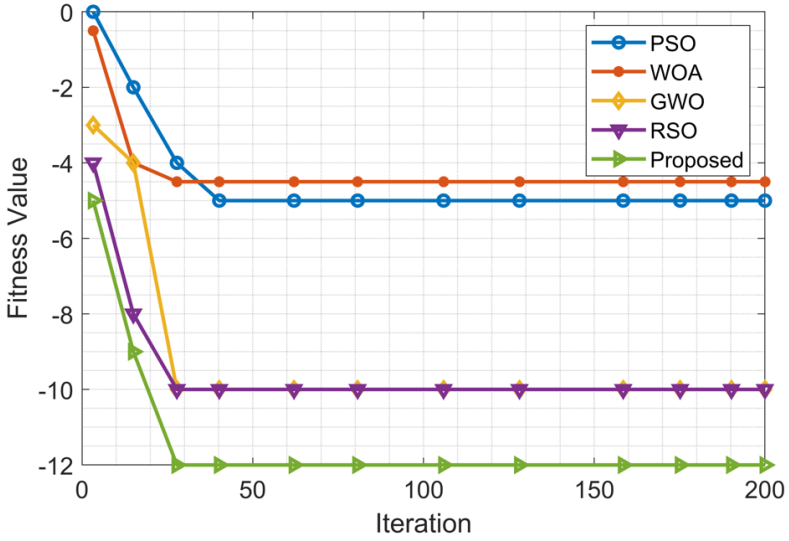

Fig. 13. State-of-art of fitness value evaluation

5. Conclusion

The work in this article is about segmenting and detecting the LC from the CT scan images and our proposed approach is based on ARaNN based ASA for detection and classification of LC images. For detecting the types of LC as HCC, ICC, HB or normal the images were preprocessed to remove the noises and was segmented utilizing the proposed FAL approach which effectively segments the Liver with DSC of 97%. To analyze the confusion matrix, the normal, ICC, HCC and HB classes shows 98.54%, 98.01%, 98.43% and 98.32% accuracy. Moreover, proposed ASO-ARaNN for LC classification approach was compared with traditional methods such as HFCNN, DL, DNN and EFCNet using the parameters like accuracy, specificity, and sensitivity. The accuracy, specificity, and sensitivity of the proposed work are 97.3%, 97.01%, and 96.8% respectively. The convergence ability of proposed ASO algorithm

is better to PSO, WOA, RSO and GWO algorithms. Our proposed approach surpasses all the other approaches in detecting and classifying the LC images.

References

1. Fan, T., Wang, G., Li, Y. and Wang, H., 2020. Ma-net: A multi-scale attention network for liver and tumor segmentation. IEEE Access, 8, pp.179656-179665.
2. Aswathy, S. U., T. Jarin, R. Mathews, LAKSHMI M. Nair, and M. Rroan. "CAD systems for automatic detection and classification of COVID-19 in nano CT lung image by using machine learning technique." Int. J. Pharm. Res 2 (2020): 1865-1870.
3. Huang, Q., Pan, F., Li, W., Yuan, F., Hu, H., Huang, J., Yu, J. and Wang, W., 2020. Differential diagnosis of atypical hepatocellular carcinoma in contrast-enhanced ultrasound using spatio-temporal diagnostic semantics. IEEE journal of biomedical and health informatics, 24(10), pp.2860-2869.
4. Wang, W., Chen, Q., Iwamoto, Y., Aonpong, P., Lin, L., Hu, H., Zhang, Q. and Chen, Y.W., 2020. Deep fusion models of multi-phase CT and selected clinical data for preoperative prediction of early recurrence in hepatocellular carcinoma. IEEE Access, 8, pp.139212-139220.
5. Mahesh, J., K. Nagamani, and T. Jarin. "Corrosion of reinforcement in concrete with fly ash and manufactured sand." Materials research innovations 23, no. 7 (2019): 413-421.
6. Sheykhmousa, M., Mahdianpari, M., Ghanbari, H., Mohammadimanesh, F., Ghamisi, P. and Homayouni, S., 2020. Support vector machine versus random forest for remote sensing image classification: A meta-analysis and systematic review. IEEE Journal of Selected Topics in Applied Earth Observations and Remote Sensing, 13, pp.6308-6325.
7. Zhu, J., Liu, Y., Zhang, Y. and Li, D., 2020. Attribute supervised probabilistic dependent matrix tri-factorization model for the prediction of adverse drug-drug interaction. IEEE Journal of Biomedical and Health Informatics, 25(7), pp.2820-2832.
8. Li, Z. and Xia, Y., 2020. Deep reinforcement learning for weakly-supervised lymph node segmentation in CT images. IEEE Journal of Biomedical and Health Informatics, 25(3), pp.774-783.
9. Dong, X., Zhou, Y., Wang, L., Peng, J., Lou, Y. and Fan, Y., 2020. Liver cancer detection using a hybridized fully convolutional neural network based on deep learning framework. IEEE Access, 8, pp.129889-129898.
10. Sun, C., Xu, A., Liu, D., Xiong, Z., Zhao, F. and Ding, W., 2019. Deep learning-based classification of liver cancer histopathology images using only global labels. IEEE journal of biomedical and health informatics, 24(6), pp.1643-1651.
11. Yan, Q., Wang, B., Zhang, W., Luo, C., Xu, W., Xu, Z., Zhang, Y., Shi, Q., Zhang, L. and You, Z., 2020. Attention-guided deep neural network with multi-scale feature fusion for liver vessel segmentation. IEEE Journal of Biomedical and Health Informatics, 25(7), pp.2629-2642.
12. Tran, S.T., Cheng, C.H. and Liu, D.G., 2020. A multiple layer U-Net, U n-Net, for liver and liver tumor segmentation in CT. IEEE Access, 9, pp.3752-3764.
13. Devi, R.M. and Seenivasagam, V., 2020. Automatic segmentation and classification of liver tumor from CT image using feature difference and SVM based classifier-soft computing technique. Soft Computing, 24, pp.18591-18598.
14. Zhang, Y., Jiang, B., Wu, J., Ji, D., Liu, Y., Chen, Y., Wu, E.X. and Tang, X., 2020. Deep learning initialized and gradient enhanced level-set based segmentation for liver tumor from CT images. IEEE Access, 8, pp.76056-76068.
15. Meng, Z., Zhao, Z., Li, B., Su, F., Guo, L. and Wang, H., 2020. Triple up-sampling segmentation network with distribution consistency loss for pathological diagnosis of cervical precancerous lesions. IEEE Journal of Biomedical and Health Informatics, 25(7), pp.2673-2685.
16. Balagourouchetty, L., Pragatheeswaran, J.K., Pottakkat, B. and Ramkumar, G., 2019. GoogLeNet-based ensemble FCNet classifier for focal liver lesion diagnosis. IEEE journal of biomedical and health informatics, 24(6), pp.1686-1694.
17. Sann, S.S., Win, S.S. and Thant, Z.M., 2021. An analysis of various image pre-processing techniques in butterfly image. International Journal for Advance Research and Development, 6(1), pp.1-4.
18. Leiva, Victor, and Gaurav Dhiman. "Archery algorithm: A novel stochastic optimization algorithm for solving optimization problems." energy 19 (2022): 22.
19. Dehghani, M. and Trojovský, P., 2022. Hybrid leader based optimization: a new stochastic optimization algorithm for solving optimization applications. Scientific Reports, 12(1), p.5549.
20. Cheng, Min-Yuan, and DoddyPrayogo. "A novel fuzzy adaptive teaching–learning-based optimization (FATLBO) for solving structural optimization problems." Engineering with Computers 33 (2017): 55-69.
21. Hashim, F.A. and Hussien, A.G., 2022. Snake Optimizer: A novel meta-heuristic optimization algorithm. Knowledge-Based Systems, 242, p.108320.
22. Fu, H., Shi, H., Xu, Y. and Shao, J., 2022. Research on Gas Outburst Prediction Model Based on Multiple Strategy Fusion Improved Snake Optimization Algorithm With Temporal Convolutional Network. IEEE Access, 10, pp.117973-117984.
23. Zheng, Weimin, Senyuan Pang, Ning Liu, Qingwei Chai, and LindongXu. "A Compact Snake Optimization Algorithm in the Application of WKNN Fingerprint Localization." Sensors 23, no. 14 (2023): 6282.
24. Huma, Zil E., ShahidLatif, Jawad Ahmad, ZebaIdrees, AnasIbrar, ZhuoZou, FehaidAlqahtani, and FatmahBaothman. "A hybrid deep random neural network for cyberattack detection in the industrial internet of things." IEEE access 9 (2021): 55595-55605.

25. Latif, S., Idrees, Z., Zou, Z. and Ahmad, J., 2020, August. DRaNN: A deep random neural network model for intrusion detection in industrial IoT. In 2020 international conference on UK-China emerging technologies (UCET) (pp. 1-4). IEEE.
26. Alahmari, S., Yonbawi, S., Racharla, S., Lydia, E.L., Ishak, M.K., Alkahtani, H.K., Aljarbouh, A. and Mostafa, S.M., 2023. Hybrid Multi-Strategy Aquila Optimization with Deep Learning Driven Crop Type Classification on Hyperspectral Images. Comput. Syst. Sci. Eng., 47(1), pp.375-391.